Vacuum-ultraviolet emission from high-pressure xenon and argon excited by high-current relativistic electron beams*

H. A. Koehler, L. J. Ferderber, D. L. Redhead, and P. J. Ebert
Lawrence Livermore Laboratory, University of California, Livermore, California 94550
(Received 13 August 1973)

High pressure Xe and Ar were excited by high-current relativistic-electron bursts. The spectral and temporal characteristics of the uv continua, centered near 1700 Å in Xe and 1260 Å in Ar, were measured. The maximum of the Xe spectral distribution shifted from 1690 ± 9 to 1710 ± 9 Å, and the spectral width decreased from 150 ± 3 to 110 ± 3 Å when the pressure was raised from 2 to 34 atm. The shift of the Ar continuum centered at 1260 ± 9 Å was negligible and the spectral width decreased from 130 ± 3 to 90 ± 3 Å when the pressure was raised from 2 to 61 atm. Exponential time constants for the buildup and decay of the Xe and Ar continua were obtained. They are characterized by a $p^{-1.5}$ pressure dependence below 3 atm. Pressure-independent decay time constants of 4 ± 1, 16 ± 2.5, and about 280 nsec were obtained for Xe at high pressure. For Ar the pressure-independent decay time constants were 6 ± 1.5, 30 ± 5, and about 230 nsec. The efficiency for conversion of electron kinetic energy to uv energy was 10 ± 4% in Xe and 15 ± 7% in Ar.

I. INTRODUCTION

Emission of vacuum-ultraviolet continuum radiation from noble gases has been observed under many experimental conditions. The emission has been studied when gases were excited by electrical discharges,[1-6] microwave discharges,[7-9] uv photons,[10] and high-energy ionizing radiations.[6,11-15] Studies have been made of emission characteristics of the liquid[16-18] and solid[16,17,19] phases and from the gas as a function of pressure.[1-15] Most of the experiments with gases were conducted at pressures below 1 atm. Experimental results indicated that the emission characteristics depended on both gas pressure and mode of excitation.

The continuum arises from radiative decay of excited diatomic molecules to the repulsive molecular ground state of the normally monatomic gas. Formation of excited molecules is a result of collisions involving excited atomic species. Mulliken[20] has estimated the potential curves for the molecular states of Xe. Similar curves have been reported for Ar.[21]

The apparent potential of the noble gases as high-power uv lasing media was first noted by Basov and co-workers, who reported stimulated emission from liquid Xe excited by relativistic electrons.[18,19] Experimental evidence of lasing in similarly excited high-pressure Xe gas was first reported by the authors[15] and subsequently by others.[22,23] These results, together with theoretical predictions that short-wavelength lasers are efficient for producing laser fusion[24] have stimulated much of the current interest in noble-gas systems.

Preliminary experiments with relativistic-electron excitation of high-pressure Xe gas have shown that the emission is predominantly a continuum centered near 1700 Å with a radiative lifetime of about 2×10^{-8} sec.[15] A more detailed investigation of the characteristics of the uv continuum emissions of Ar and Xe at pressures ranging from 0.2 to 65 atm is the subject of this report. Preliminary accounts of this work have been given previously.[25]

II. EXPERIMENT

The following emission characteristics of high-pressure Ar and Xe were measured: spectrum as a function of pressure; continuum output intensity as a function of time and pressure; and efficiency for conversion of electron energy to uv emission energy.

A. Experimental apparatus

Figure 1 is a schematic diagram of the experimental apparatus consisting of an electron source, a cell for containing high-pressure gas, and film and photodiode uv sensors. Oscilloscopes recorded photodiode output.

1. Electron sources

Two electron sources were used, a Febetron 705 and a Febetron 706.[26] The Febetron 705 can generate an electron burst with a peak current of 7×10^3 A at 2 MV peak potential. The full width at half-maximum (FWHM) of the burst is 50 nsec.

The average electron excitation energy is 1.3 MeV. In preliminary measurements with the 2-MV source, an inductive-current pickup loop, located between the electron gun and the entrance window of the gas cell, monitored the electron beam current. This loop was calibrated with a Faraday cup located 10 cm from the electron gun, where electrons would normally enter the gas cell. With the Faraday cup at this location, the highest achievable current was 2×10^3 A. A Si-PIN detector located 2 m from the electron gun simultaneously monitored the x-ray output.[27] Figure 2 compares signals from the Faraday cup, the beam monitor, and the Si-PIN x-ray monitor. For experiments at higher excitation current, the pickup loop was removed and the gas cell moved closer to the electron gun. The entrance window was then located approximately 4 cm from the electron gun. The current increased to 5×10^3 A. In this configuration, only the x-ray monitor was used. All spectra and efficiency data were obtained with the 2-MV machine.

The Febetron 706 can generate an electron burst with a peak current of 7×10^3 A at 0.6-MV peak potential. The burst FWHM is 1.6 nsec. The average electron excitation energy with the 706 was 0.1 MeV. The burst shape was measured with a 50-Ω coaxial Faraday cup.[28] Figure 3 compares the Faraday cup output with that of a plastic scintillator coupled to a planar photodiode. The latter was used to monitor the x-ray output of the 0.6-MV electron source. A long-duration (~25 nsec) low-intensity contribution to the electron pulse

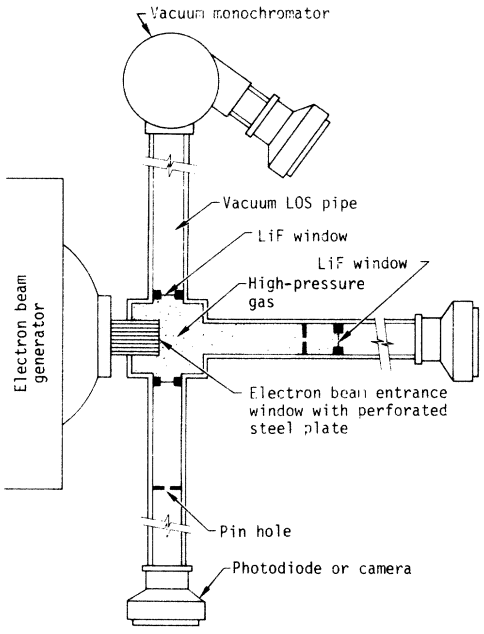

FIG. 1. Schematic diagram of experimental apparatus.

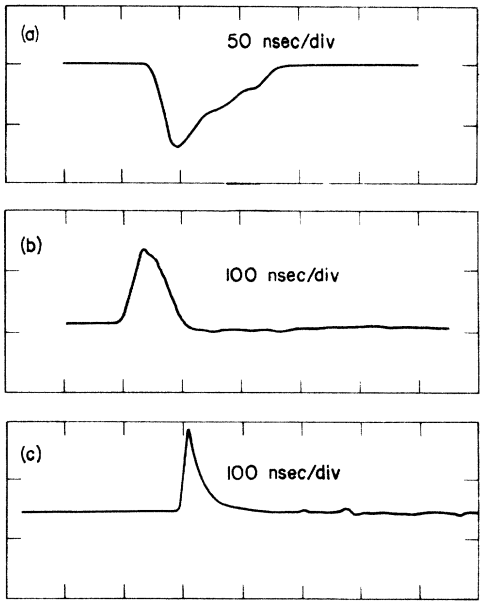

FIG. 2. 1.3-MeV electron burst measured with (a) a Faraday cup and (b) an inductive pickup loop. The Si-PIN x-ray monitor output is shown in (c). The amplitude scale is in arbitrary units.

(0.5% of peak) is not apparent in either of the traces shown in Fig. 3 but was easily observable with a NaI (Tl) scintillator coupled to a photodiode. This detector integrated the x-ray flux delivered in a time much less than its 230-nsec decay time.[29] Approximately 5% of the total x-ray energy was in the low-current portion of the pulse. All data on the buildup and decay of uv intensity were obtained with the 0.6-MV machine.

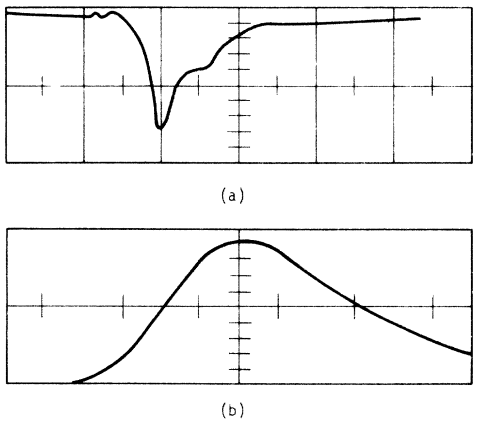

FIG. 3. 0.1-MeV electron burst (a) measured with a coaxial Faraday cup and (b) monitored with a plastic scintillator coupled to a planar photodiode. The time scale is 2 nsec/cm for both traces. The amplitude scale is in arbitrary units.

2. Gases

High-purity Ar and Xe were used. Impurity concentrations were measured with a gas chromatograph. In Ar, the impurities and their measured concentrations were: H_2, 1 ppm; N_2, 4 ppm; Kr, 1 ppm; Xe, 0.1 ppm; CH_4, 1 ppm. The O_2 concentration could not be measured. The studies of Gedanken *et al.*[30] have shown that it is essential to remove higher Z noble gases from Ar. To remove Xe from the gas cell, the cell was flushed several times with Ar that was filtered by a molecular sieve cooled in a solid CO_2 and Freon bath. In Xe the impurities and their concentrations were: H_2, 0.5 ppm; N_2, 15 ppm; O_2, 1.5 ppm; Ar, 2 ppm; Kr, 65 ppm; CH_4, 0.3 ppm.

High pressures were measured with a calibrated Heise gauge that could be read with an accuracy of 1.0 psi (0.07 atm). A Wallace and Tiernan gauge with an accuracy of 0.10 psi was used for low-pressure (< 3 atm) experiments.

The gases were at an ambient temperature of 22°C in these experiments. The gas pressure returned to its initial value within seconds of each burst, indicating that the initial gas temperature was close to ambient temperature.

3. Gas cell

The gas cell is an improved version of the one described previously.[15] It was constructed of stainless steel, with metal seals for the steel electron entrance window and the LiF uv windows. The 2.2-cm-diam electron entrance window was 0.013-cm thick. To prevent large deformation at high pressure, the electron entrance window was supported by a perforated steel plate having a geometrical transmission factor of 0.6. Two LiF uv windows were located perpendicular to the electron-beam axis so that the gas volume next to the electron entrance window was observable. The distance between the electron-beam axis and these windows was 5 cm. This was adequate to minimize radiation damage to the LiF. A third LiF window was mounted along the beam axis at a distance of 20 cm from the electron-beam entrance window. All LiF windows were 2-mm thick and 1.27 cm in diameter. The diameter of the viewing aperture at each window was 0.8 cm. Vacuum line-of-sight (LOS) pipes extended from the LiF windows to the optical sensors. A vacuum of approximately 10^{-3} Torr was maintained in the LOS for signal measurements. Background measurements were made with air at 1 atm pressure in the LOS. Allowing for scattering of the 1.3-MeV electrons in the gas, the observable excited volume along the perpendicular LOS was approximately 1.3 cm^3. Along the parallel LOS, most of the excited gas was observable. This was verified from pinhole-camera photographs.

The gas cell was leak-free up to 100 atm and was not a source of contaminants in these experiments. This was experimentally established by exciting Xe repeatedly at 30 shots/h. The uv power varied ±3% about the average power in an experiment using 48 bursts. A decrease in uv output at a fixed pressure invariably indicated that the electron entrance window was punctured or that a LiF window had cracked.

4. Optical sensors

Characteristics of the Ar and Xe emission continua were determined using a vacuum monochromator with either uv-sensitive film or a photodiode as well as with photodiodes alone. Spectra were obtained with a 0.5-m Saya-Namayoka-type vacuum monochromator having a 1200-lines/mm grating blazed at 1500 Å. Relative grating reflectivity was unknown and the spectra are uncorrected for wavelength variations in grating reflectivity. In first-order diffraction, the dispersion was 17 Å/mm. The focal plane of a lensless camera was located at the monochromator

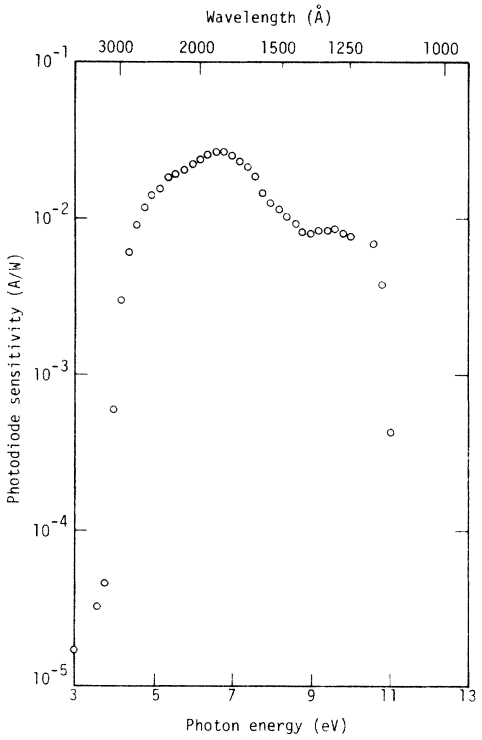

FIG. 4. Absolute sensitivity of a Cs_2Te photodiode used in these experiments. All photodiodes used were cross calibrated against this diode.

exit slit position for film recording of time-integrated spectra.[31] The monochromator was centered at 1260 Å for Ar and at 1700 Å for Xe. Wavelength bands 500 Å wide were observable. The spectra were indexed with a hydrogen discharge lamp and with identified absorption lines present in the Ar and Xe continua.

Most spectral data were obtained with Kodak 101-01 uv sensitive film. This film is sensitive up to 4000 Å. Film density was read with a Joyce-Loebl scanning microdensitometer. The linear region of the density-vs-log exposure curve for this film was determined with a Xe flashlamp and a step-wedge. This was cross-checked by comparing the film density to the photodiode output. The monochromator entrance-slit width was narrowed with increasing pressure to prevent film saturation.

With the exit slit in place and the photodiode attached to the monochromator, the Xe emission in 34-Å-wide bands was also measured in 25-Å increments from 1600 to 1900 Å.

A 0.5-m Bauch and Lomb monochromator with a 600-lines/mm grating blazed at 5000 Å was used to check for emissions between 3000 and 7000 Å. Polaroid ASA 10 000 speed film, located in the focal plane of the monochromator, was used as an optical sensor. To obtain film exposure, the monochromator entrance slit had to be opened to 2 mm and the 2-MV machine had to be pulsed several times.

The uv emission rate was measured with an ITT F4115 planar photodiode. This type of diode has a 2.5-mm-thick MgF_2 window and a 1.9-cm-diam Cs_2Te photocathode.[32] The sensitivity as a function of wavelength is shown in Fig. 4. With

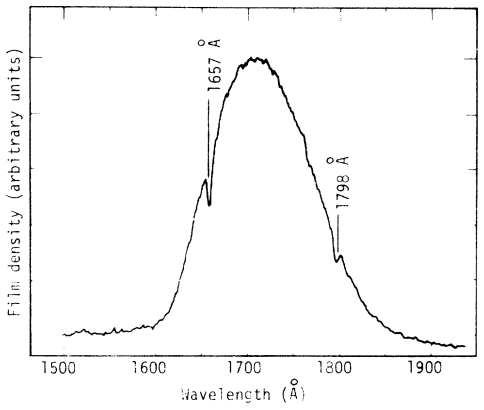

FIG. 5. Time-integrated emission spectrum of Xe at 34 atm. 1.3-MeV electrons excited the gas. The densitometer recording is uncorrected for grating reflectivity and wavelength-dependent absorption by the unexcited gas.

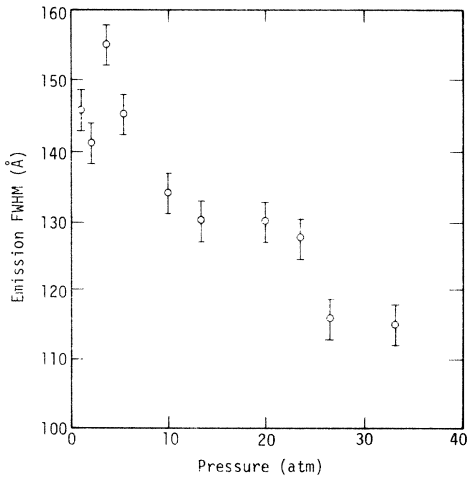

FIG. 6. Pressure dependence of emission FWHM of the Xe continuum. Wavelength values are uncorrected for grating reflectivity and wavelength-dependent absorption by the unexcited gas. Error is indicated by the length of each vertical bar.

8-kV anode bias, this type of diode can deliver a linear current of 15 A into 50 Ω. To assure linearity, the output current was never allowed to exceed 5 A. This was done by placing pinholes in the LOS between the gas cell and the photodiodes.

5. *Recording oscilloscopes*

Tektronix 519, 585, and 7904 oscilloscopes recorded the photodiode and monitor signals that were fed through at most 100-nsec lengths of RG-8 cable. The bandwidth of the 519 and 7904 os-

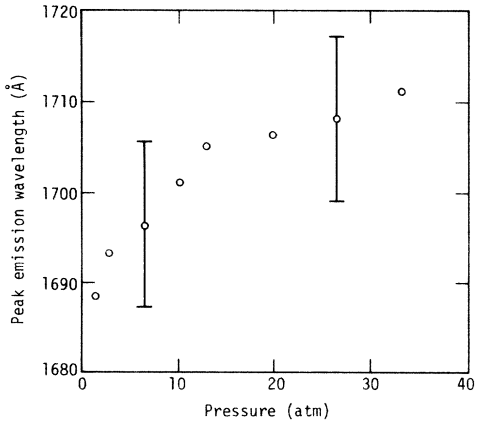

FIG. 7. Pressure dependence of λ_{max}, the wavelength at which the emission is a maximum in Xe. Wavelength values are uncorrected for grating reflectivity and wavelength-dependent absorption by the unexcited gas. Error is indicated by the length of each vertical bar.

cilloscope-cable-detector systems was adequate for measuring the 1.6-nsec Febetron 706 pulse. For the intensity measurements, the amplitude scale of each oscilloscope was dc calibrated and the time-base linearity was determined with a 50-MHz sine-wave generator. Care was taken to assure that the oscilloscopes recorded the signals in the linear region of the horizontal sweep. Attenuators used with the 519 and 7904 oscilloscopes were pulse calibrated.

B. Experimental results: xenon

1. *Emission spectra*

Time-integrated spectra were obtained from 2 to 34 atm pressure. A typical spectrum taken at 34 atm is shown in Fig. 5. No correction was made for the wavelength-dependent absorption by 4 cm of unexcited gas. The emission peaks at 1709 Å; absorption lines at 1657 and 1798 Å are apparent. The 1657 Å absorption line is attributed to C. The strength of this absorption could not be related to Xe gas pressure and is presumed to result from absorption by hydrocarbons deposited in the monochromator system.

The emission FWHM decreases with increasing pressure, as shown in Fig. 6. Figure 7 shows the wavelength at which the continuum is a maximum, λ_{max}, increasing with increasing pressure.

Time-resolved spectra were obtained at 10 and 20 atm using the 50-nsec excitation pulse. The shapes of the photodiode output pulses did not vary with wavelength. No difference between these spectra and those obtained with film was apparent.

In addition to the uv continuum centered near 1700 Å, very weak emissions at 3100 and 5400 Å were also observed. No other emissions were detected between the LiF cutoff at approximately 1050 and 7000 Å.

2. *Buildup and decay of uv intensity*

Time constants for the buildup and decay of the uv continuum intensity were obtained by fitting a sum of exponential terms $[I(t)=\sum_i A_i e^{-t/\tau_i}]$ to oscilloscope traces of the photodiode output pulses (Fig. 8). A negative amplitude A_i characterizes intensity buildup; a positive amplitude intensity decay. Comparison of some of these fits to oscilloscope traces are shown in Fig. 9. Table I lists the time constants and the amplitudes at several gas pressures. Figure 10 shows the time constants as a function of pressure. Table I and Fig. 10 use the fewest number of exponential terms that fit the traces to within the experimen-

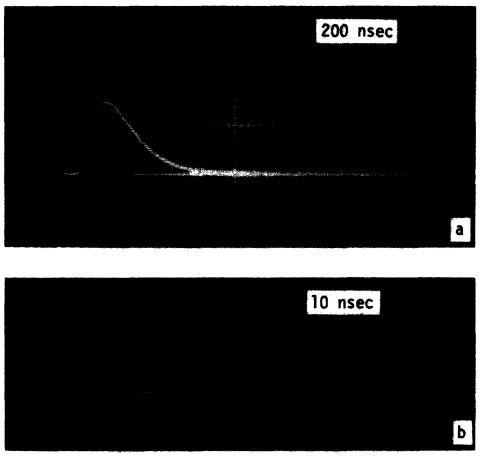

FIG. 8. Oscilloscope traces of photodiode output at (a) 0.54-atm Xe and (b) 29-atm Xe. The gas was excited by a 1.6-nsec-wide electron burst. Baselines were obtained with zero-volt signal prior to gas excitation.

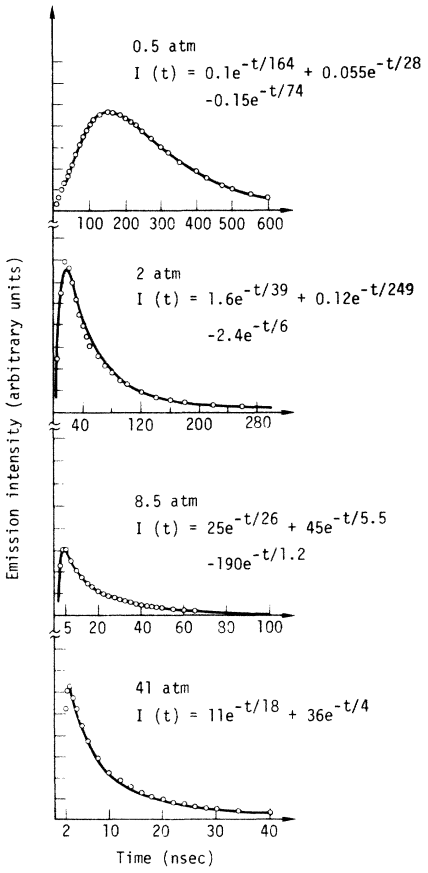

FIG. 9. Comparison of computer fits (solid lines) to points read from the oscilloscope traces (open circles) of Xe uv emission pulses. The equation giving the best fit at each gas pressure is also given. The gas was excited by a 1.6-nsec-wide electron burst.

tal error. Data obtained on a fast time scale (out to 80 nsec) were fit over a voltage range of a factor of 20–30 while data on a slow time scale (out to 500 nsec or greater) were fit over a voltage range of a factor of 50–100.

Below 3 atm, one buildup term and two decay terms were adequate to fit the data. A very fast precursor coinciding with the excitation pulse was evident at low pressure (Fig. 8). The precursor was not used in the curve fitting since it was of longer wavelength than the 1700 Å continuum. The precursor was observed with air in the LOS but not with black paper. The buildup and both decay time constants exhibit a pressure dependence of $\tau_i \sim P^{-1.5}$. At each pressure, the faster decay component had approximately one-half the amplitude of the slower decay component. The amplitudes of the buildup component and both decay components exhibit a pressure dependence of $A_i \sim P^{2.6}$.

Above 3 atm, the buildup-time constant could not be measured accurately since the buildup time was comparable to the duration of the excitation pulse. Data taken on a slow time scale were fit with three decay components. The slowest component was relatively weak and had a pressure-independent time constant of about 280 nsec. Two large-amplitude decay components were obtained from the slow and fast time scale data. The slower of these components was weakly pressure dependent to 15 atm. Above 15 atm, it was pressure independent and had a time constant of 16 nsec. The faster component had a 4-nsec time constant that was independent of pressure above 7 atm. The amplitude ratio $A_{\text{fast}} : A_{\text{slow}}$ of these decay components was approximately 2:1. This ratio was independent of pressure. The amplitudes, but not the time constants, of both components decreased rapidly with pressure above 24 atm.

To determine if the decay constants were affected by the high excitation current usually employed, some data were obtained using less than one-tenth the usual current. Although the uv intensity decreased, there was no change in the time constants.

To determine if these results were influenced by the presence of other wavelength emissions, high-pressure time constants at several pressures were also obtained with the photodiode located behind the exit slit of the vacuum monochromator. These time constants were the same as those obtained without the monochromator.

3. *Output power and efficiency*

Figure 11 shows the peak power emitted by approximately 1.3 cm^3 of excited Xe gas as a function of pressure. The observable volume was determined from densitometer scans of pinhole camera images that were obtained along both the parallel and perpendicular LOS. The power plotted in Fig. 11 was calculated from the peak output voltage of oscilloscope traces similar to those shown in Fig. 8. Detector geometry and sensitivity were known. Isotropic gas emission was

TABLE I. Time constants and amplitudes for Xe buildup and decay obtained by fitting oscilloscope traces to $I(t) = \sum_i A_i e^{-t/\tau_i}$.

Pressure (atm)	Amplitude (arbitrary units)					Time constant (nsec)				
	$-A_1$	A_2	A_3	A_4	A_5	τ_1	τ_2	τ_3	τ_4	τ_5
0.27	0.015		0.053	0.01		140		60	440	
0.54	0.15		0.055	0.1		74		28	160	
0.95	0.54		0.29	0.23		20		10	80	
1.4	1.0	0.07		0.55		12	300		49	
2.0	2.4	0.12		1.6		6	250		39	
2.7	7.1	0.4		4.0	3.8	5	250		35	10
4.1	30			8.3	9.8	3			31	8
5.4	44			17	26	2			27	4.4
8.5	190			27	48	1.2			26	5.5
13.6				26	48				23	5.5
20.4				24	52				20	4.5
29.3				32	56				13	3.5
41.0				11	36				18	4.0
42.5				9.6	20				15	3.5
47.6				3.6	9				17	4.0
54.4				1.1	2.4				15	3.5

assumed. A 20% correction was made for uv transmission through the LiF window. No correction was made for transmission through 4 cm of unexcited gas. The peak power increased with increasing pressure, reaching a maximum of 3×10^7 W at 24 atm. The power decreased with further increase in pressure. Similar behavior was observed along the parallel LOS, where most of the excited gas was observable. Along this LOS, the peak power at 24 atm was 3×10^8 W.

Emission energy was obtained from measurement of the area under each oscilloscope trace. The maximum energy emitted from the 1.3 cm^3 gas volume was 1.9 J at 24 atm. The corresponding value along the parallel LOS was 20 J.

To obtain the efficiency for conversion of electron kinetic energy to uv energy from measurements along the perpendicular LOS, the energy absorbed per unit volume of gas (W_e) was calculated from the following expression:

$$W_e = jF\gamma \left(\frac{dE}{dx}\right) \rho \,, \tag{1}$$

where j is the electron current density (1700 A/cm^2), F is the geometrical transmission of the plate supporting the electron entrance window (0.6), γ is the FWHM of the electron burst (50 nsec), dE/dx is the effective collision energy-loss rate determined by Monte Carlo calculations (~3.3 MeV/g/cm^2 in Xe,[33] and ρ is the gas density. For these experimental conditions, $W_e = 150\rho$ J/cm^3.

In the above expression, it is assumed that the gas is thin for electrons. On the basis of the Monte Carlo calculation, this is a reasonable assumption up to approximately 25-atm gas.

Along the perpendicular LOS, the uv energy density divided by the electron energy density was 0.1.

Along the parallel LOS, we assumed that all of the transmitted burst energy is absorbed by the gas. For an average electron energy of 1.3 MeV, a transmitted current of 3000 A, and a 50-nsec FWHM, the absorbed energy is 2×10^2 J.

The same efficiency value of 0.1 is obtained along the parallel LOS when the uv energy is divided by the electron burst energy. This value was independent of pressure below 24 atm.

C. Experimental results: argon

1. *Emission spectra*

Time-integrated emission spectra were obtained between 2 and 61 atm. A typical spectrum, taken at 34 atm, is shown in Fig. 12. The emission peaks at 1265 Å. No correction was made for the 15% variation in the transmission of LiF across the Ar emission continuum or for the wavelength-dependent absorption by the unexcited gas. Absorption lines of H, C, N, and O are apparent in Fig. 12. While there was very little shift in the λ_{max} with pressure, spectral narrowing with increasing pressure was noted. This is shown in Fig. 13. In addition to the 1260-Å continuum, very weak emissions were found at 1900 and 2180 Å. The 1900-Å peak emission intensity was larger than the 2180-Å peak emission. We were able to correlate a significant decrease of the 1900-Å emission intensity with the passage of Ar through a dry-ice-cooled molecular sieve. This suggests that the 1900-Å continuum is impurity related. Water is known to emit in this wavelength region.

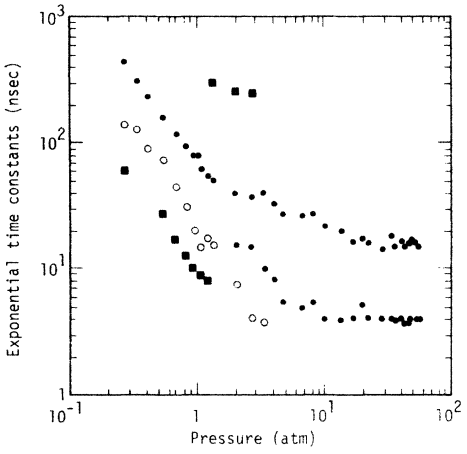

FIG. 10. Time constants for Xe intensity as a function of pressure. ○, buildup-time constants; ●, time constants of the strong decay components; ■, time constants of the weak decay components.

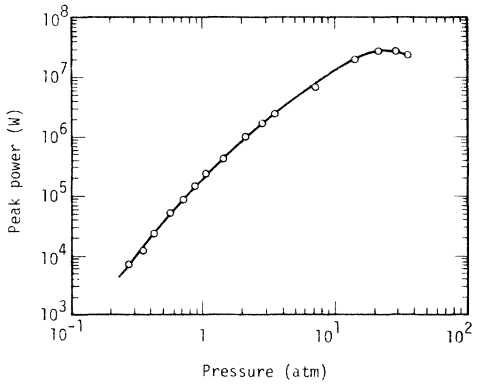

FIG. 11. Peak power of Xe emission from 1.3 cm^3 of gas as a function of pressure. The data points were corrected for transmittance of the LiF window. No correction was made for the absorption by the unexcited gas.

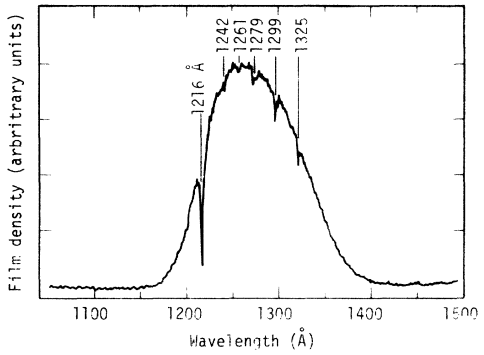

FIG. 12. Time-integrated emission spectrum of Ar at 34 atm. 1.3-MeV electrons excited the gas. The densitometer recording is uncorrected for grating reflectivity, wavelength variation of LiF transmittance, and the wavelength-dependent absorption by the unexcited gas.

2. *Buildup and decay of uv intensity*

Time constants for the buildup and decay of the Ar uv continuum intensity were obtained using the same fitting procedure as for Xe. Table II lists the time constants and amplitudes above 6 atm. Figure 14 is a plot of the time constants as a function of pressure. Figure 15 shows oscilloscope recordings of the photodiode output at several gas pressures. The very fast precursor was not included in the curve fitting procedure since it was not part of the 1260-Å continuum. This was determined by using a series of filters (air, quartz, KBr) with the photodiode that identified the wavelength of the precursor to be between approximately 1800 and 2300 Å. The amplitude of this emission increased linearly as the pressure was raised from 0.7 to 7 atm. This precursor was not affected by the addition of the dry-ice-cooled molecular sieve to the gas-fill system. This suggests that the precursor results from the 2180-Å continuum.

In the pressure range 0.15–2 atm, the buildup and decay time constants exhibit a pressure dependence of $\tau_i \sim P^{-1.5}$. Below 0.6 atm, one buildup and one decay term were used to fit each oscilloscope trace. Above 0.6 atm, it was necessary to introduce an additional decay term. The faster of the two decays maintains the $P^{-1.5}$ pressure dependence. The slower decay decreases with pressure up to approximately 2 atm.

TABLE II. Time constants and amplitudes for Ar buildup and decay obtained by fitting oscilloscope traces to $I(t) = \sum_i A_i e^{-t/\tau_i}$.

Pressure (atm)	Amplitude (arbitrary units) A_1	A_2	Time constant (nsec) τ_1	τ_2
6.8	6	5.5	6	37
10	20	8	6	32
14	22	10	6.5	35
17	30	13	6.5	37
20	30	15	5.5	30
24	27	16	6.0	30
30	36	24	5.5	25
37	42	18	7.0	30
44	45	17	6.5	36
51	42	22	6.0	25
58	40	17	6.5	28
65	46	20	6.5	28

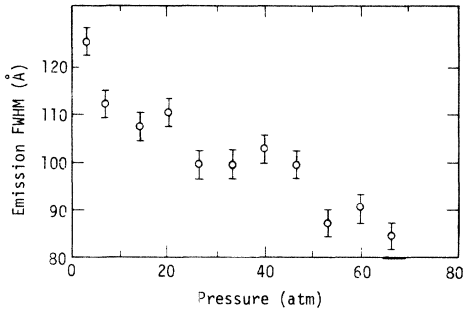

FIG. 13. Pressure dependence of the emission FWHM of the Ar continuum. Error is indicated by the length of the vertical bar.

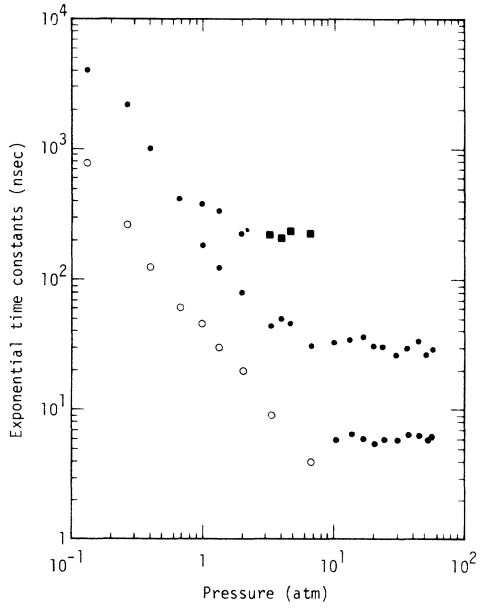

FIG. 14. Time constants for Ar intensity as a function of pressure. ○, buildup-time constants; ●, time constants of the strong decay components; ■, time constants of the weak decay components.

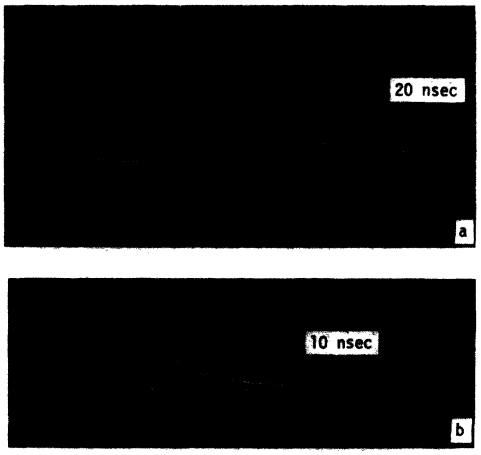

FIG. 15. Oscilloscope traces of photodiode output at (a) 6.3-atm Ar and (b) 34-atm Ar. The gas was excited by a 1.6-nsec-wide electron burst. Baselines were obtained with zero-volt signal prior to gas excitation.

Above 2 atm, two decay components were used to fit each trace. Below 7 atm, the slower decay constant appeared to be pressure independent, with a value of approximately 230 nsec. The other component decreased with increasing pressure asymptotically approaching a pressure-independent value of 30 nsec near 7 atm. Above this pressure, 30-nsec and 6-nsec decay constants were used to fit the oscilloscope traces. The latter decay constant was also independent of pressure. The ratio of the amplitudes of these high-pressure components, $A_{\text{fast}} : A_{\text{slow}}$, was approximately 3:1 and was independent of pressure.

3. *Output power and efficiency*

Figure 16 shows the peak power emitted by approximately 1.3 cm^3 of excited gas as a function of pressure. Correction was made for the LiF window transmission (50%). No corrections were made for transmission through 4 cm of unexcited gas. The peak power increased with pressure, reaching a maximum of 6×10^7 W at 61 atm. The uv output energy at this pressure was 3 J. The electron energy density, estimated from Eq. (1), was 16 J/cm^3. This results in an efficiency for conversion of electron kinetic energy to uv energy of 15%.

D. Experimental error

1. *Random error*

Random error in measurement of spectra, of time constants and their corresponding amplitudes, and of the output power and efficiency for conversion of electron energy to uv energy was estimated from known error sources listed in Table III. The effects of these sources of error on the measurements are discussed below.

The measurement of distance on the uv film had a typical error of ±0.05 mm, corresponding to a wavelength uncertainty of ±0.85 Å. This error was negligible in determining $\lambda_{\max}$. The uncertainty in locating the most dense part of the film was accurate to ±0.5 mm, or 8.5 Å. In determining the spectral FWHM, the largest error was in measuring the positions of half-intensity (density 0.3 below the maximum film density). The error in these measurements was ±0.15 mm, resulting in a ±3-Å uncertainty.

The major error sources in time constants and amplitude measurements were the reading of each oscilloscope trace and the curve-fitting procedure. The relative error in each time constant was estimated from the expression:

$$\frac{\Delta\tau}{\tau} = \left\{ \left[\left(\frac{\Delta V_1}{V_1} \right)^2 + \left(\frac{\Delta V_2}{V_2} \right)^2 \right] \left(\frac{\tau}{t} \right)^2 + \left(\frac{\Delta t}{t} \right)^2 \right\}^{1/2} ,$$

where V_1 is the vertical oscilloscope deflection at t_1, V_2 is the deflection at a later time t_2, and $t = t_2 - t_1$. The absolute uncertainty in V_1, V_2, and t was ±0.03 cm (0.5 trace width). Because of this

TABLE III. Summary of random experimental errors.

Measurement	Random error (%) Xe	Ar
Photodiode sensitivity	±10	±30
Oscilloscope attenuators	±5	±5
Oscilloscope dc calibration	±2	±2
Oscilloscope trace reading for ~1-cm deflection	±3	±3
Geometrical correction factor	±6	±6
Ultraviolet window transmission	±5	±10
Electron current integration	±20	±20
dE/dx	±20	±20
Excited-gas volume	±20	±20

error in V_1 and V_2, the region where minimum uncertainty in τ is obtained falls in the range $0.3 \leq \tau/t \leq 3$. Since the time constants were assumed to be independent, the uncertainty in a faster decay constant can be obtained from this equation after incorporating in V_1 and V_2 additional uncertainties that result from the subtraction of a slower decay component. The estimated error in the slower high-pressure decay constants (16 nsec in Xe, 30 nsec in Ar) is ±15%. The error in the faster high-pressure decay constants (4 nsec in Xe, 6 nsec in Ar) is ±20%.

The uncertainty in the buildup-time constant depended on the durations of both the excitation pulse and the uv buildup. At low pressure, the excitation pulse was short compared to the buildup time, and the buildup-time constants could be determined to within ±20%. At higher pressures ($P > 3$ atm), the excitation time and the uv rise time were comparable, and the uncertainty in the buildup time constant exceeded 100%.

The uncertainties in the amplitudes for the buildup and decay depended on the uncertainties in the time constants and the absolute uncertainty in $t = 0$. In our analysis, $t = 0$ was chosen to be at the breakout of the uv emission pulse, and the error in determining this was at most ±0.3 nsec. The ±15 and ±20% errors in the time constants and the ±0.3-nsec timing error resulted in an error of ±40% in the amplitude of the fast component and an error of ±25% in the amplitude of the slow component. The uncertainty in the buildup amplitude was ±25% at low pressure but exceeded ±100% at high pressure.

Output power and efficiency are absolute measurements in which the errors are determined by uncertainties in photodiode sensitivity (±10% for Xe and ±30% for Ar), oscilloscope attenuators (±5%), oscilloscope calibration (±2%), film reading (±3%), optical geometry factor (±6%), LiF transmission (±5% for Xe and ±10% for Ar). Adding these in quadrature gives errors in both the peak power and the uv output energy of ±14% for Xe and ±32% for Ar.

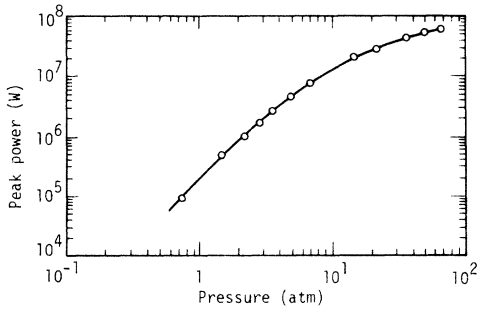

FIG. 16. Peak power of Ar emission from 1.3 cm^3 of gas as a function of pressure. The data points were corrected for average transmittance of the LiF window. No correction was made for absorption by the unexcited gas.

The error in efficiency depended upon uncertainties in the output energy, the excitation volume, and the accuracy in calculating the energy deposited per unit volume. The volume is accurate to ±20%. Contributing to the error in the energy deposited per unit volume are uncertainties in electron current density (±20%) and dE/dx (±20%). All of these are added in quadrature to give an error in the efficiency of ±37% for Xe and ±47% for Ar.

2. *Systematic error*

In addition to the uncertainties in Table III, sources of systematic error were present. These are discussed below.

The reflectivity of the grating used in these experiments was not measured. A wavelength dependence of the grating reflectivity would result in an error in the absolute value of λ_{max} and the FWHM of the continua. The reflectivity of a similar blaze angle grating[13] varied from 19 to 22% across the Ar continuum and from 18 to 13% across the Xe continuum. Correcting a typical Xe spectrum (27 atm) for such grating reflectively increases λ_{max} approximately 25 Å and increases the FWHM approximately 15 Å. Applying the correction to an Ar spectrum (68 atm) results in a decrease in λ_{max} of 6 Å and leaves the FWHM unchanged. If $\Delta R/\Delta\lambda$ is relatively constant and small over the wavelength range of the continua, the effect of such corrections on the relative pressure dependence of λ_{max} (Fig. 7) and FWHM (Figs. 6 and 13) is negligible. The measured LiF window transmittance exhibited a wavelength variation that was small compared with the published variations in reflectivity. Spectra were not corrected for either of these variations.

No systematic study of the effect of impurities on these results was undertaken. However, experiments with Xe having 2-ppm total impurity concentration gave the same time constants as those with the gas used for most of these experiments. Absorption lines in the continua were the only evidence of impurities. The strength of the absorption could not be correlated with gas pressure and is presumably the result of uv absorption by impurities in the monochromator.

A simplistic calculation assuming adiabatic heating gives an instantaneous temperature increase of 3×10^3 °K for 1.3-MeV electron excitation. No long-term temperature increase was observed. The effects of instantaneous heating on

the experimental results are unknown. It should also be pointed out that identical time-constant results were obtained when less than one-tenth the excitation current was used.

System time response consisting of photodiode rise time (< 0.5 nsec), oscilloscope rise time (0.3 nsec), and cable response (< 0.5 nsec) caused negligible signal degradation to the shortest decay times reported. This is evidenced by the short duration of the precursor.

The 1.6-nsec FWHM excitation burst from the Febetron 706 had a 25-nsec long contribution that was approximately 0.5% of the peak electron current. To determine if this shape excitation pulse distorted the Xe uv output pulse shape, the excitation pulse was convolved with the sum of exponentials at 20 atm. Except for a time shift, the convolution was identical to the sum of exponentials. For this reason, negligible systematic error is attributed to the excitation pulse shape.

Transmittance of 1700-Å continuum energy through 13 cm of unexcited Xe gas at various pressures is shown in Fig. 17. Each point is proportional to the spectral energy transmitted. Since all of the absorption could occur over a very short length, a linear extrapolation to obtain a correction factor for the 4-cm gas-cell absorption path could be in error by as much as a factor of approximately 15 at 56 atm. Therefore, all output power data are uncorrected for this effect. In Ar, self-absorption through 13 cm of unexcited gas was 11% at the highest attainable pressure.

III. DISCUSSION

These experimental results can be discussed in light of potential curves for the molecular states of Xe[20] and Ar[21] together with kinetic models of the formation and decay of excited molecules.[4,21,34,35]

Figure 18 illustrates some of the more important collision and radiative processes that occur in a noble gas excited by relativistic electrons. Many of these processes have been incorporated in the various models. In Fig. 18, formation or dissociation of an excited species by collision is illustrated by a solid line. The collision partner is given along the line. Radiative transitions are indicated by waved lines. Spontaneous dissociation of bound excited states (such as suggested by Mulliken[20] at points of potential curve crossing) and unbound states is indicated by a dashed line. A double star indicates a higher level of atomic or molecular excitation and a single star, a lower level of excitation. Formation of atomic and mo-

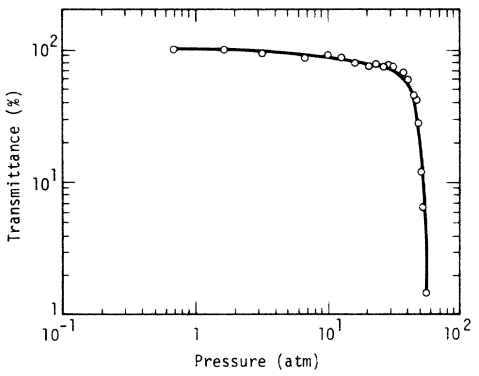

FIG. 17. Pressure dependence of narrow beam transmittance of a 13-cm column of Xe gas for the 1700-Å continuum produced by 1.3-MeV electron excitation of Xe at 7 atm.

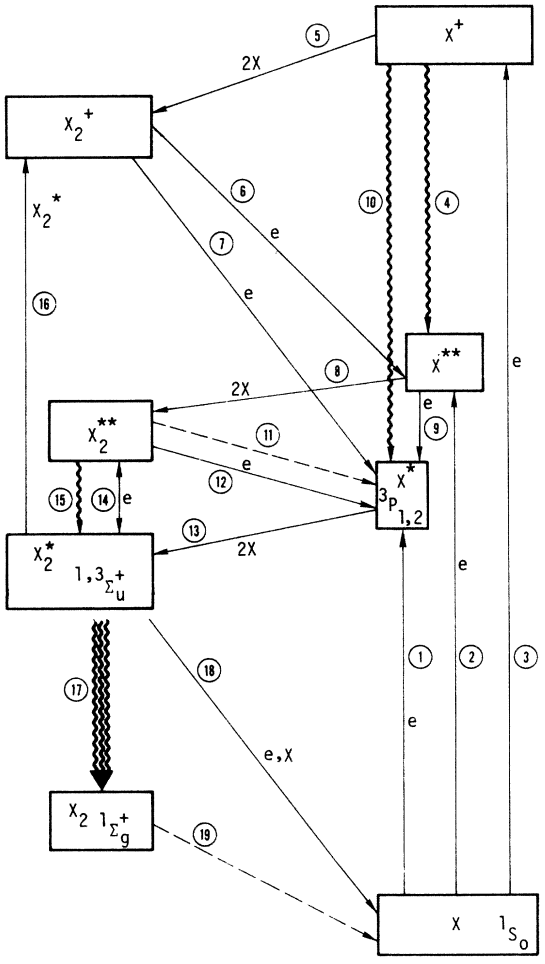

FIG. 18. Schematic diagram of some possible phenomena in an electron-excited noble gas. Solid lines represent collisional relaxation or excitation with the particles indicated. Waved lines represent radiative deexcitation. Dashed lines represent spontaneous dissociation.

lecular ions is included because relativistic electrons lose energy mainly by ionizing collisions.

A. Spectra

Pathways of possible radiative decay are given along lines 4, 10, 15, and 17 in Fig. 18. Not shown are electronic transitions in excited ions that result mainly in visible emissions.

Virtually all of the energy emitted was in the uv continua centered near 1700 Å in Xe and 1260 Å in Ar. These continua (line 17) are attributed to radiative transitions from the $^1\Sigma_u^+$ and $^3\Sigma_u^+$ states to the $^1\Sigma_g^+$ molecular ground state. The narrowing of the continua with increasing pressure results from absorption in a ground-state population (X_2) that increases with increasing pressure. This should also result in an increase in λ_{max} with increasing pressure. Quantitative interpretation of this increase, observed in Xe but not in Ar, requires accurate shapes of the potential curves for the ground state and the radiative states. Radiative transitions from higher excited molecular states to the $^1\Sigma_u^+$ and $^3\Sigma_u^+$ states have been suggested by Mulliken[20] and have been observed in Ar by Arai and Firestone.[36] We could not detect these transitions, which are approximately 10 000 Å wavelength in Ar and approximately 20 000 Å in Xe because our apparatus was sensitive in the 1050–7000-Å region.

No emission at wavelengths shorter than the uv continua were observed from either gas. This indicates resonant trapping of photons from atomic transitions and the absence of photons from radiative decay of higher energy molecular states to the ground state.

The lack of strong, longer wavelength uv and visible emissions indicates rapid collisional deexcitation of the large initial ion population to lower excited atomic or molecular states. Viecelli[35] has suggested that the long wavelength bands observed in Ar^{37} (1950 Å), Kr^{37} (2200 Å), and Xe^{35} (3000 Å) result from radiative recombination of electrons and atomic ions (lines 4 and 10). The 3040-Å band in Xe and the 2180-Å band in Ar, observed in our experiments, could be evidence of these transitions.

B. Time constants and amplitudes

Buildup- and decay-time constants and their relative amplitudes were obtained by fitting a sum of exponentials to the experimental data. For both Xe and Ar, the high-pressure ($P > 20$ atm) decay constants were independent of pressure. These results together with the spectra suggest that two spectrally unresolvable molecular states ($^1\Sigma_u^+$, $^3\Sigma_u^+$) decay independently to the molecular ground state ($^1\Sigma_g^+$). Since singlet-singlet transitions are more probable than triplet-singlet transitions, it is reasonable to assign the short decay (4 nsec in Xe, 6 nsec in Ar) to the former and the long decay (16 nsec in Xe, 30 nsec in Ar) to the latter. It should be emphasized that identical time constants were obtained both with and without the monochromator. The pressure-independent time constants of approximately 280 nsec in Xe and approximately 230 nsec in Ar could result from infrared transitions (line 15) suggested by Mulliken.[20]

In Xe above 24 atm, the amplitudes of the decay components decreased with increasing pressure but maintained the 2:1 ratio. This decrease cannot be explained on the basis of electron energy absorption outside the viewing aperture. It is also difficult to ascribe this to quenching since a deexcitation reaction including two excited molecules (line 16) or one excited molecule and an electron (line 18) would result in nonexponential decay. Additionally, a deexcitation reaction involving a single excited molecule and a ground-state atom (line 18) would give pressure-dependent decay constants. Excellent fits to the oscilloscope traces were obtained with pressure-independent, exponential decay constants. Therefore, it is believed that self-absorption by ground-state molecules arising from two-body collisions accounts for the amplitude decrease. This is also reasonable in view of the very small transmittance of Xe at high pressure (Fig. 17) and the shift and narrowing of the spectra with increasing pressure.

In Ar, the amplitudes appear to reach a maximum at the highest attainable pressure, suggesting a behavior similar to that in Xe. Because of safety limitations on the gas cell, we were unable to investigate this phenomenon in Ar gas of higher density. In Ar, the ratio of the amplitudes of the fast and slow decay components was approximately 3:1. This implies that for both Ar and Xe, the concentration of triplet molecules was approximately twice the concentration of singlet molecules.

The decay constants in Ar can be discussed in light of the Xe time constants since the over-all behavior of the two gases is strikingly similar. Time constants at low pressure have a $P^{-1.5}$ pressure dependence that is associated with the formation of radiative molecules (lines 6, 7, 8, 11, 12, and 13). Since the reaction rates along line 5 (Ref. 38) and lines 4 and 10 (Ref. 35) are greater than the rates[5] along both lines 8 and 13, the excited radiative molecules can be considered as products of reactions of ionic molecules and excited atoms that are formed essentially during the

excitation (lines 1, 2, and 3). Above 3 atm, the pressure-dependent decay constants approach their pressure-independent values.

The very fast precursors apparent in the oscilloscope recordings of the photodiode outputs (Figs. 8 and 15) result from photons of longer wavelength than the uv continua arising from molecular decay. The precursors are indicative of very fast processes such as radiative recombination[35] along lines 4 and 10.

The pressure-dependent time constants reported here agree with those reported by Boucique and Mortier[5] for Xe at $P<0.7$ atm. Their pressure-independent time constant of 0.5 μsec does not compare with any of our pressure-independent time constants. More recent publications, of experiments similar to those described earlier,[15] report pressure-dependent time constants leading to single molecular lifetimes of Xe_2^* of 16 nsec[39] and 130 nsec.[40] The 16-nsec value is in excellent agreement with our results although our 4-nsec time constant was not found. Perhaps the 130-nsec value obtained by Wallace *et al.*[40] was strongly affected by use of a photocathode having much greater sensitivity in the 3000-Å region than in the 1700-Å region.[41]

The pressure-dependent time constants of Ar are consistent with time constants reported by Boucique and Mortier,[5] Thonnard and Hurst,[14] and by Colli.[3] We did not observe the very long (~3 μsec) pressure-independent time constant reported by these investigators.

C. Output power and efficiency

The maximum power density observed for the Xe continuum using the 2-MV electron source was 2.4×10^7 W/cm^3 at 24 atm. At 37 atm, the peak power density decreased to 1.9×10^7 W/cm^3. This behavior parallels that of the amplitudes of the decay components. The efficiency of 10% agrees with the value determined by Stewart *et al.*[6] for proton excitation.

The maximum power density observed for the Ar continuum using the 2-MV electron source was 5×10^7 W/cm^3 at 61 atm. The efficiency of 15% is in reasonable agreement with the value of 29% reported by Stewart *et al.*[6]

ACKNOWLEDGMENTS

The authors thank G. Clough for performing the mechanical design and construction of much of the apparatus and for his assistance in obtaining some of the data. The help of S. Stribling, D. Jones, and V. Gregory in the mechanical aspects of these experiments is also gratefully acknowledged.

---

*Work performed under the auspices of the U. S. Atomic Energy Commission.

[1]Y. Tanaka, J. Opt. Soc. Am. 45, 710 (1955).
[2]R. E. Huffman, J. C. Larrabee, and Y. Tanaka, Appl. Opt. 4, 1581 (1965).
[3]L. Colli, Phys. Rev. 95, 892 (1954).
[4]D. S. Smith and R. Turner, Can. J. Phys. 41, 1949 (1963).
[5]R. Boucique and P. Mortier, J. Phys. D 3, 1905 (1970).
[6]T. E. Stewart, G. S. Hurst, T. E. Bortner, J. E. Parks, F. W. Martin, and H. L. Weidner, J. Opt. Soc. Am. 60, 1290 (1970).
[7]Y. Tanaka and M. Zelikoff, J. Opt. Soc. Am. 44, 254 (1954).
[8]P. G. Wilkinson and Y. Tanaka, J. Opt. Soc. Am. 45, 344 (1955).
[9]P. G. Wilkinson and E. T. Byram, Appl. Opt. 4, 581 (1965).
[10]C. G. Freeman, M. J. McEwan, R. F. C. Claridge, and L. F. Phillips, Chem. Phys. Lett. 10, 530 (1971).
[11]T. D. Strickler and E. T. Arakawa, J. Chem. Phys. 41, 1783 (1964).
[12]Y. Mikawa, J. Opt. Soc. Am. 55, 569 (1965).
[13]G. S. Hurst, T. E. Bortner, and T. D. Strickler, Phys. Rev. 178, 4 (1969).
[14]N. Thonnard and G. S. Hurst, Phys. Rev. A 5, 1110 (1972).
[15]H. A. Koehler, L. J. Ferderber, D. L. Redhead, and P. J. Ebert, Appl. Phys. Lett. 21, 198 (1972).
[16]J. Jortner, L. Meyer, S. A. Rice, and E. G. Wilson, J. Chem. Phys. 42, 4250 (1965).
[17]N. G. Basov, E. M. Balashov, O. V. Bogdankevitch, V. A. Danilychev, G. N. Kashnikov, N. P. Lantzov, and D. D. Khodkevitch, J. Lumin. 2, 834 (1970).
[18]N. G. Basov, V. A. Danilychev, and Yu. M. Popov, Kvantovaya Elektronika 1, 29 (1971) [Sov. J. Quantum Electron. 1, 18 (1971)].
[19]N. G. Basov, O. V. Bogdankevitch, V. A. Danilychev, A. G. Devyatkov, G. N. Kashnikov, and N. P. Lantsov, Zh. Eksp. Teor. Fiz. Pizma Red. 7, 404 (1968) [JETP Lett. 7, 317 (1968)].
[20]R. S. Mulliken, J. Chem. Phys. 52, 5170 (1970).
[21]D. C. Lorents and R. E. Olson, Stanford Research Institute Semi-Annual Technical Report No. 1, December, 1972 (unpublished).
[22]J. B. Gerardo and A. W. Johnson, in Proceedings of the IEEE/OSA Conference on Laser Engineering and Applications, Washington, D.C., May, 1973 (unpublished).
[23]P. W. Hoff, J. C. Swingle, and C. K. Rhodes, in Ref. 22.
[24]J. W. Shearer and J. J. Duderstadt, UCRL Report No. UCRL-74094 (unpublished).

[25]L. J. Ferderber, H. A. Koehler, and P. J. Ebert, Bull. Am. Phys. Soc. 18, 710 (1973).
[26]Reference to a company or product name does not imply approval or recommendation of the product by the University of California or the U. S. AEC to the exclusion of others that may be suitable.
[27]R. W. Kuckuck, UCRL Report No. UCRL-51011, 1971 (unpublished).
[28]P. J. Ebert and D. R. Lasher, Rev. Sci. Instrum. 37, 964 (1966).
[29]L. M. Bollinger and G. E. Thomas, Rev. Sci. Instrum. 32, 1044 (1961).
[30]A. Gedanken, J. Jortner, B. Raz, and A. Szoke, J. Chem. Phys. 57, 3456 (1972).
[31]G. A. Clough and H. A. Koehler, Rev. Sci. Instrum. 43, 1836 (1972).
[32]G. B. Fisher, W. E. Spicer, P. C. McKernan, V. F. Pereskok, and S. J. Wanner, Appl. Opt. 12, 799 (1973).
[33]M. J. Berger and S. M. Seltzer, NASA Report No. SP-169, 1968 (unpublished). Unpublished calculations carried out with program ETRAN-15.
[34]E. V. George and C. K. Rhodes, UCRL Report No. UCRL-74516 (unpublished).
[35]J. A. Viecelli, UCRL Report No. UCRL-51374, 1973 (unpublished).
[36]S. Arai and R. F. Firestone, J. Chem. Phys. 50, 4575 (1969).
[37]B. Krawetz and C. Rhodes, UCRL Report No. UCRL-73777, 1972 (unpublished).
[38]D. Smith, A. G. Dean, and I. C. Plumb, J. Phys. B 5, 2134 (1972).
[39]D. J. Bradley, M. H. R. Hutchinson, and H. Koetser, Opt. Commun. 7, 187 (1973).
[40]S. C. Wallace, R. T. Hodgson, and R. W. Dreyfus, Appl. Phys. Lett. 23, 22 (1973).
[41]*Typical Absolute Spectral Response Characteristics of Photoemissive Devices* (ITT Industrial Laboratories, Ft. Wayne, Ind., 1970); *Typical Photocathode Spectral Response Characteristics* (RCA Electronics Components, Harrison, N. J., 1970).

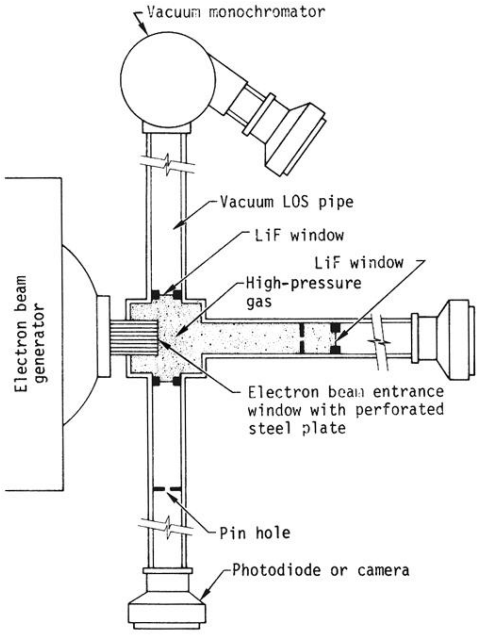

FIG. 1. Schematic diagram of experimental apparatus.

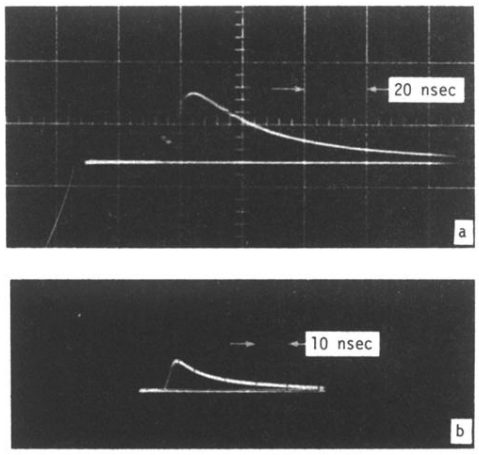

FIG. 15. Oscilloscope traces of photodiode output at (a) 6.3-atm Ar and (b) 34-atm Ar. The gas was excited by a 1.6-nsec-wide electron burst. Baselines were obtained with zero-volt signal prior to gas excitation.

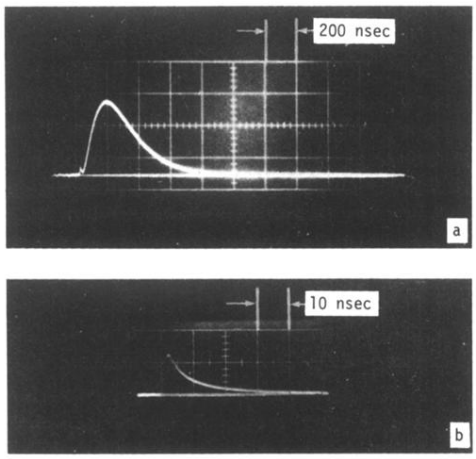

FIG. 8. Oscilloscope traces of photodiode output at (a) 0.54-atm Xe and (b) 29-atm Xe. The gas was excited by a 1.6-nsec-wide electron burst. Baselines were obtained with zero-volt signal prior to gas excitation.